

Dynamical dimerization phase in Jaynes-Cummings lattices

Rubén Peña,¹ Felipe Torres,^{2,3} and Guillermo Romero^{1,3,*}

¹*Departamento de Física, Universidad de Santiago de Chile (USACH),
Avenida Ecuador 3493, 9170124, Santiago, Chile*

²*Departamento de Física, Facultad de Ciencias, Universidad de Chile, Casilla 653, Santiago, Chile 7800024*

³*Center for the Development of Nanoscience and Nanotechnology, Estación Central, 9170124, Santiago, Chile*
(Dated: November 26, 2019)

We report on an emergent dynamical phase of a strongly-correlated light-matter system, which is governed by dimerization processes due to short-range and long-range two-body interactions. The dynamical phase is characterized by the spontaneous symmetry breaking of the translational invariance and appears in an intermediate regime of light-matter interaction between the resonant and dispersive cases. We describe the quench dynamics from an initial state with integer filling factor of a finite-sized array of coupled resonators, each doped with a two-level system, by using an effective Hilbert space that accounts for resonant polaritonic states. This procedure allows us to demonstrate and characterize the emergent dynamical phase via time-averaged quantities, such as fluctuations in the number of polaritons per site and linear entropy. Our findings reveal that intrinsic two-body interactions and the lattice topological structure govern the dynamical phase.

I. INTRODUCTION

The development of technology encompasses a broad range of opportunities to harness quantum phenomena. For instance, it is possible to manipulate light-matter quasiparticles or polaritons which have new properties such as stimulated scattering [1, 2], lasing [3–5], parametric amplification [6–8], and superfluidity [9, 10]. These characteristics can be used to enhance the experimental realization of polaritonic devices, such as semiconductor microcavities, where the coupling between quantum-well excitons and cavity photons gives rise to hybrid light-matter quasiparticles [11]. In the microwave regime, superconducting circuits based on Josephson junctions also allow to harness light-matter interaction for simulating strongly correlated phenomena with light [12–22]. The underlying physics of light-matter based quantum simulators is governed by the Jaynes-Cummings-Hubbard (JCH) model [23–25] which describes the dynamics of coupled-resonator arrays (CRAs), each doped with a two-level system (TLS). In this case, the manipulation of polaritonic excitations locally depends on the detuning between the light and matter frequencies but also is largely influenced by the lattice structure. As the detuning increases from the resonant to the dispersive regime, the system transits from the Mott-insulating state characterized by the hybridization of light and matter states to a superfluid phase of photons [23–30].

In this work, we demonstrate by using numerical simulation and an analytic model that during the phase transition from the Mott-insulating to superfluid state, a dynamical dimerization phase (DDP) emerges, which is characterized by the spontaneous symmetry breaking of the translational invariance. As dynamical dimerization, we refer to the dynamics of a finite-sized Jaynes-Cummings (JC) lattice that exhibits resonances related

to the two-sites JC lattice. In order to demonstrate the existence of DDP, first, we analyze the quench dynamics of few-body Jaynes-Cummings lattices. In particular, we consider a quantum quench from an initial state with integer filling factor in a closed Jaynes-Cummings dimer, which has been proven useful to simulating second-order like phase transitions from the Mott-insulating to superfluid phase [31]. Here, we introduce an effective Hilbert space in the two-excitations subspace using the criterion of discarding higher energy polaritonic states, which are out-of-resonance over the evolution [27, 32]. This description allows us quantitative explanations for time-averaged quantities such as fluctuations in the number of polaritons per site and linear entropy. Besides, the computational cost is substantially diminished by using a reduced effective Hilbert space. As we extend the quench dynamics to complex finite-sized CRAs, we demonstrate the emergence of DDP, which is governed by intrinsic two-body interactions in the Jaynes-Cummings lattice. Our findings could be tested with state-of-the-art quantum technologies such as trapped ions and superconducting circuits.

This paper is organized as follows. In Sec. II, we introduce the JCH model and the polariton mapping. In Sec. III, we describe the quench protocol for the JCH dimer. Here, we provide quantitative explanations of time-averaged order parameters using an effective Hilbert space. In Sec. IV, we highlight the emergence of a dynamical dimerization phase as we extend the one-dimensional Jaynes-Cummings lattice to three and four sites. Finally, in Sec. V, we present our concluding remarks.

II. THE MODEL

The Jaynes-Cummings-Hubbard model [23–25] describes a lattice of L interacting coupled QED resonators, each supporting a single mode of the electromagnetic field which interacts with a two-level system. This situation

* guillermo.romero@usach.cl

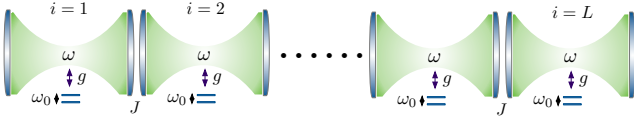


FIG. 1. Schematic representation of a Jaynes-Cummings-Hubbard lattice. Each resonator supports a single mode of the electromagnetic of frequency ω , which interacts with a two-level system of frequency ω_0 . This interaction is represented by the coupling strength g . The interaction between cavities is characterized by the hopping parameter J .

is schematically shown in Fig. 1. The JCH Hamiltonian reads ($\hbar = 1$)

$$H_{\text{JCH}} = \sum_i H_i^{\text{JC}} - \sum_{\langle i,j \rangle} J_{ij} (a_i^\dagger a_j + a_j^\dagger a_i), \quad (1)$$

where $a_i (a_i^\dagger)$ is the annihilation (creation) bosonic operator at the i th lattice site, J_{ij} is the photon-photon hopping amplitude which takes values $J_{ij} = J$ if two sites of the lattice are connected and $J_{ij} = 0$ otherwise. Also, $H_i^{\text{JC}} = \omega a_i^\dagger a_i + \omega_0 \sigma_i^+ \sigma_i^- + g(\sigma_i^+ a_i + \sigma_i^- a_i^\dagger)$ is the Jaynes-Cummings (JC) Hamiltonian [33] where $\sigma_i^+ (\sigma_i^-)$ is the raising (lowering) operator acting on the i th TLS eigenbasis $\{|\downarrow\rangle_i, |\uparrow\rangle_i\}$, and ω , ω_0 , and g are the resonator frequency, TLS frequency, and light-matter coupling strength, respectively.

In the resonant regime, $\Delta = \omega_0 - \omega = 0$, the hybridization of the light-matter yields to localized polariton excitations (Mott-insulator phase), while in the dispersive regime, $\Delta \gg g$, the system is dominated by photonic excitation behavior (superfluid phase) [23, 24]. This phase transition can also be described as a transition driven by the photon blockade effect from the Mott-insulator phase, where the intersite polariton exchange is forbidden, so effectively $J_{ij} = 0$, to a superfluid phase dominated by a

uniform photon hopping $J_{ij} = J$, in both cases, there is no cavity-embedded effect involved. As we demonstrate in Sec. IV, the intermediate regime of light-matter interaction, which we define in the range $1 < \Delta/g < 10$, can be identified by the parameter $k_i = J(\sum_j \nu_j)/L$ with L the number of nonlinear coupled resonators, J the hopping parameter, and ν_j the connectivity of node j . Notice that $k_i = 0$ for the resonant case and $k_i = J$ for the dispersive case. This way, the origin of translational symmetry breaking can be explained by introducing a local order parameter of μ -th phase Ψ_i^μ , with $\mu = (\text{I, II, III})$ represents the resonant, intermediate, and dispersive case, respectively. Indeed, $\Psi_i^{\text{I}}(k_i) = \Psi^{\text{I}}(0)$, and $\Psi_i^{\text{III}}(k_i) = \Psi^{\text{III}}(J)$, which means that in the resonant and dispersive regimes there is translational invariance. Since the order parameter shows a spatial dependence in an intermediate regime $\Psi_i^{\text{II}}(k_i)$, then translational symmetry is broken. As a consequence, a *dynamical dimerization phase* will happen due to intrinsic two-body interactions and the connectivity of each lattice site.

The Hamiltonian (1) preserves the total number excitations (polaritons) described by the operator $\mathcal{N} = \sum_{i=1}^L (a_i^\dagger a_i + \sigma_i^+ \sigma_i^-)$. The i th node of the lattice in Fig. 1 is described by the JC Hamiltonian H_i^{JC} whose eigenstates define the upper (+) and lower (-) polaritonic basis $|n, \pm\rangle_i = \gamma_{n\pm} |\downarrow, n\rangle_i + \rho_{n\pm} |\uparrow, n-1\rangle_i$ with energies $E_n^\pm = n\omega + \Delta/2 \pm \chi(n)$. Here, $\chi(n) = \sqrt{\Delta^2/4 + g^2 n}$, $\rho_{n+} = \cos(\theta_n/2)$, $\gamma_{n+} = \sin(\theta_n/2)$, $\rho_{n-} = -\gamma_{n+}$, $\gamma_{n-} = \rho_{n+}$, $\tan \theta_n = 2g\sqrt{n}/\Delta$, and the detuning parameter $\Delta = \omega_0 - \omega$. Also, one introduces the i th polaritonic creation operators as $P_i^{\dagger(n,\alpha)} = |n, \alpha\rangle_i \langle 0, -|$, where $\alpha = \pm$ and we identify $|0, -\rangle \equiv |\downarrow, 0\rangle$ and $|0, +\rangle \equiv |\emptyset\rangle$ being a ket with all entries equal to zero, that is, it represents an unphysical state. These identifications imply $\gamma_{0-} = 1$ and $\gamma_{0+} = \rho_{0\pm} = 0$.

Using the above defined polaritonic basis, the Hamiltonian (1) can be rewritten as [23, 27].

$$H = \sum_{i=1}^L \sum_{n=1}^{\infty} \sum_{\alpha=\pm} E_n^\alpha P_i^{\dagger(n,\alpha)} P_i^{(n,\alpha)} - \sum_{\langle i,j \rangle} J_{ij} \left[\sum_{n,m=1}^{\infty} \sum_{\alpha,\alpha',\beta,\beta'=\pm} t_n^{\alpha\alpha'} t_m^{\beta\beta'} P_i^{\dagger(n-1,\alpha)} P_i^{(n,\alpha')} P_j^{\dagger(m,\beta)} P_j^{(m-1,\beta')} + \text{H.c.} \right], \quad (2)$$

where the matrix elements $t_n^{\alpha\alpha'} = \sqrt{n} \gamma_{(n-1)\alpha} \gamma_{n\alpha'} + \sqrt{n-1} \rho_{(n-1)\alpha} \rho_{n\alpha'}$. The first term in Eq. (2) stands for the local polaritonic energy with an anharmonic spectrum and gives rise to an effective on-site polaritonic repulsion. This is analog to the on-site photon repulsion in the Bose-Hubbard model [34]. The last term in Eq. (2) represents the polariton hopping between resonators. This interaction also allows the interchange of polaritonic species of one or both sites involved [23, 27, 32], leading to a quite involve quantum dynamics.

A detailed understanding of the equilibrium properties

of the JCH model (2) resorts on approximated analytical solutions [35] or numerical approaches such as density matrix renormalization group [36–39]. In nonequilibrium situations one can understand the underlying physics using the time-evolving block decimation algorithm [40–42], or simplifying the description by means of effective Hilbert spaces [32, 43–47]. The latter is particularly appropriate for studying the quench protocol presented in this article.

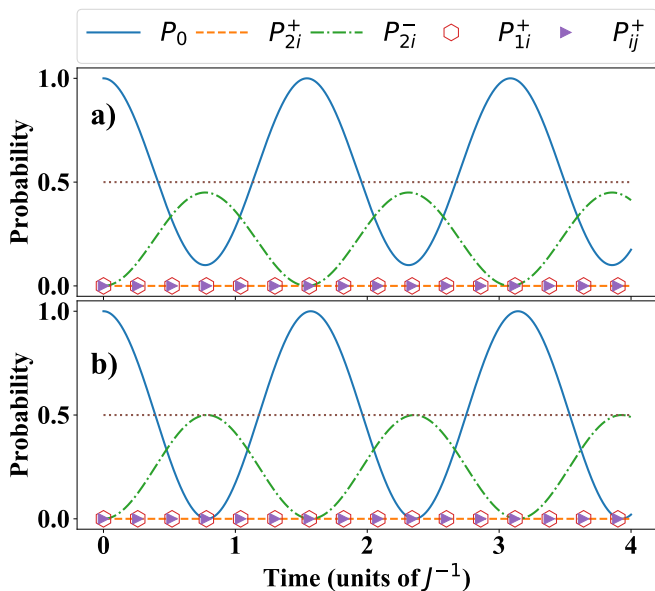


FIG. 2. Populations of states $|\psi_0\rangle$, $|\psi_2^\pm\rangle_i$, $|\psi_1^\pm\rangle_i$, and $|\psi_1^\pm\rangle_{ij}$, defined in the main text, as a function of time. The dimer is initialized in the state $|\psi_0\rangle$, parameters are $g = 10^{-2}\omega$, $J = 10^{-4}\omega$, where ω is the resonator frequency, and we consider up to 5 Fock states per resonator. (a) $\Delta = 5g$, (b) $\Delta = 50g$. Horizontal dotted lines have been added as a guide to the eye.

III. QUENCH DYNAMICS IN A JAYNES-CUMMINGS-HUBBARD DIMER

In this section, we describe a particular quench protocol presented in Ref. [31] and its effects on the quantum dynamics of the JCH dimer. Also, we provide quantitative explanations of time-averaged quantities such as fluctuations in the number of polaritons per site and linear entropy using an effective Hilbert space. In Sec. IV we will show that the underlying physics of the quench dynamics allow us to understand the emergent *dynamical dimerization phase*.

The quench protocol consists of the following steps:

Step 1.—At $J_{ij} = 0$, initialize the system in the state $|\psi_0\rangle = |1, -\rangle_i |1, -\rangle_j$, for a particular value of the detuning Δ on each node of the dimer. This initial state has an integer filling factor with one polariton per site. The subindexes i and j refer to the leftmost and rightmost node of the dimer, respectively, and $|1, -\rangle_i = \gamma_{1-} |\downarrow, 0\rangle_i + \rho_{1-} |\downarrow, 1\rangle_i$.

Step 2.—Let the system evolve under the JCH Hamiltonian (1) ($J_{ij} = J \neq 0$) for a time $\tau = J^{-1}$, and compute time-averaged order parameters such as the variance of the number of polaritons per site $\text{Var}(n_i) = \frac{1}{\tau} \int_0^\tau (\langle n_i^2 \rangle - \langle n_i \rangle^2) dt$, where $n_i = a_i^\dagger a_i + \sigma_i^+ \sigma_i^-$, or the linear entropy $E = \frac{1}{\tau} \int_0^\tau S_{\rho_i}(t) dt$, where $S_{\rho_i}(t) = 1 - \text{Tr}(\rho_i^2)$, and ρ_i the reduced density matrix of the leftmost or rightmost site of the JC dimer.

Step 3.—Iterative process of 1 and 2.

The non-equilibrium dynamics described above allows

to simulating second-order like phase transition captured via the $\text{Var}(n_i)$, see Ref. [31], which is analog to the adiabatic dynamics studied in Ref. [23]. Also, the simulated phase transitions in a JCH lattice can be characterized via linear entropy, as shown in this article, which implies that the emergent DDP is independent of the choice of order parameter.

Effective Hilbert space.—In order to introduce an effective description of the system dynamics, it is useful to consider the JCH Hamiltonian written in the polaritonic basis, see Eq. (2). Starting from the initial state $|\psi_0\rangle = |1, -\rangle_i |1, -\rangle_j$, the JCH Hamiltonian (2) may lead to processes such as the exchange of polaritonic species, or the interchange of polaritonic species of one or both sites involved (i, j). In this case, the full quantum dynamics should involve all states within the two-excitations subspace, which we define as $\{|\psi_0\rangle = |1, -\rangle_i |1, -\rangle_j, |\psi_2^\pm\rangle_i = |2, \pm\rangle_i |0, -\rangle_j, |\psi_2^\pm\rangle_j = |0, -\rangle_i |2, \pm\rangle_j, |\psi_1^\pm\rangle_i = |1, +\rangle_i |1, -\rangle_j, |\psi_1^\pm\rangle_j = |1, -\rangle_i |1, +\rangle_j, |\psi_1^\pm\rangle_{ij} = |1, +\rangle_i |1, +\rangle_j\}$. However, interchange of polaritonic excitations can be neglected under the conditions $\{|E_2^+ - 2E_1^-, |2E_1^+ - E_2^-, |E_1^+ + E_1^- - E_2^-\} \gg J$, which results in fast oscillating contributions, and we can apply the rotating-wave approximation [23, 27, 32]. Figure 2 clearly shows that the interchange of polaritonic species is suppressed over the evolution. Here we plot the populations of above defined states as a function of time, starting from the initial state $|\psi_0\rangle$. We identify populations as $P_0 = |\langle \psi_0 | \psi(t) \rangle|^2$, $P_{2i}^\pm = |\langle \psi_2^\pm | \psi(t) \rangle|^2$, $P_{1i}^+ = |\langle \psi_1^+ | \psi(t) \rangle|^2$, and $P_{ij}^+ = |\langle \psi_1^+ | \psi(t) \rangle|^2$. Due to the symmetry of the JC dimer, it is clear that $P_{2j}^\pm = |\langle \psi_2^\pm | \psi(t) \rangle|^2 = P_{2i}^\pm$ and $P_{1j}^+ = |\langle \psi_1^+ | \psi(t) \rangle|^2 = P_{1i}^+$ (not shown in Fig. 2). In this work, we carry out numerical simulations with the quantum toolbox in Python QuTiP [48, 49].

Since the interchange of polaritonic species is suppressed over the evolution, we can introduce an effective Hilbert space involving states of the lower polaritonic branch $\mathcal{H}_I = \{|\psi_0\rangle, |\psi_2^-\rangle_i, |\psi_2^-\rangle_j\}$ for describing the quench dynamics. In this case, the effective Hamiltonian reads ($\hbar = 1$)

$$H_{\text{eff}} = \begin{pmatrix} a & b & b \\ b & c & 0 \\ b & 0 & c \end{pmatrix}, \quad (3)$$

where $a = 2E_1^-$, $b = -Jt_1^- t_2^-$, $c = E_2^-$, and $t_1^- t_2^- = \cos(\theta_1/2)(\sqrt{2} \cos(\theta_1/2) \cos(\theta_2/2) + \sin(\theta_1/2) \sin(\theta_2/2))$. Thus, the full dynamics can be solved analytically by diagonalizing the above 3×3 matrix.

Starting from the initial condition $|\psi_0\rangle = |1, -\rangle_i |1, -\rangle_j$, the wave function at time t reads

$$|\psi(t)\rangle = c_0(t)|\psi_0\rangle + c_{2i}^-(t)|\psi_2^-\rangle_i + c_{2j}^-(t)|\psi_2^-\rangle_j, \quad (4)$$

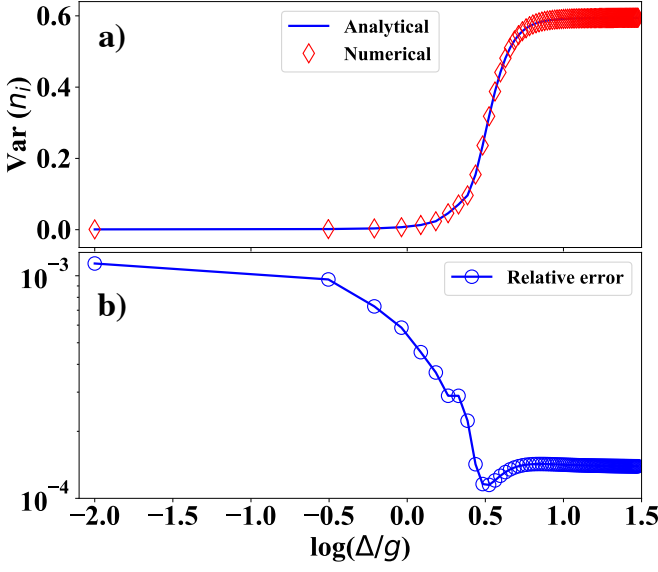


FIG. 3. (a) Time-averaged order parameter $\text{Var}(n_i)$ as a function of $\log_{10}(\Delta/g)$. (b) Comparison between the analytical and numerical predictions of $\text{Var}(n_i)$ (cf. Eq. (6)). We use parameters $g = 10^{-2}\omega$, $J = 10^{-4}\omega$, where ω is the resonator frequency.

where the probability amplitudes are

$$c_0(t) = \frac{1}{\alpha_+ - \alpha_-} (\alpha_+ e^{-it\lambda_+} - \alpha_- e^{-it\lambda_-}), \quad (5a)$$

$$c_{2i}^-(t) = c_{2j}^-(t) = \frac{1}{\alpha_+ - \alpha_-} (e^{-it\lambda_+} - e^{-it\lambda_-}), \quad (5b)$$

and we define the coefficients $\lambda_{\pm} = (a + c \pm \sqrt{8b^2 + (a - c)^2})/2$, $\alpha_{\pm} = (a - c \pm \sqrt{8b^2 + (a - c)^2})/2b$.

Time-averaged order parameters.—Given the wave function (4), we can analytically compute time-averaged order parameters such as the variance of the number of polaritons per site $\text{Var}(n_i) = \frac{1}{\tau} \int_0^{\tau} (\langle n_i^2 \rangle - \langle n_i \rangle^2) dt$, where $n_i = a_i^\dagger a_i + \sigma_i^+ \sigma_i^-$, or the linear entropy $E = \frac{1}{\tau} \int_0^{\tau} S_{\rho_i}(t) dt$, where $S_{\rho_i}(t) = 1 - \text{Tr}(\rho_i^2)$, and ρ_i the reduced density matrix of the leftmost or rightmost site of the JC dimer. Thus, the time-averaged variance reads

$$\text{Var}(n_i) = \frac{4b^2}{\Omega_0^2} \left[1 - \frac{J}{\Omega_0} \sin\left(\frac{\Omega_0}{J}\right) \right], \quad (6)$$

where we define $\Omega_0 = \sqrt{8b^2 + (a - c)^2}$.

Figure 3(a) shows the behavior of $\text{Var}(n_i)$ as a function of $\log_{10}(\Delta/g)$ calculated from the full numerics (red diamonds) and the analytical prediction (continuous blue line) in Eq. (6). We see a good agreement between both predictions as the relative error shows in Fig. 3(b). Also, Eq. (6) allows us to predict the asymptotic behavior of $\text{Var}(n_i)$ as the detuning increases, $\Delta/g \rightarrow \infty$. In this case, the spectrum of the lower (upper) polaritonic branch becomes harmonic with eigenenergies $E_n^- \approx n\omega_R$ ($E_n^+ \approx n\omega_R + \Delta$), where $\omega_R = \omega - g^2/\Delta$, thus allowing the

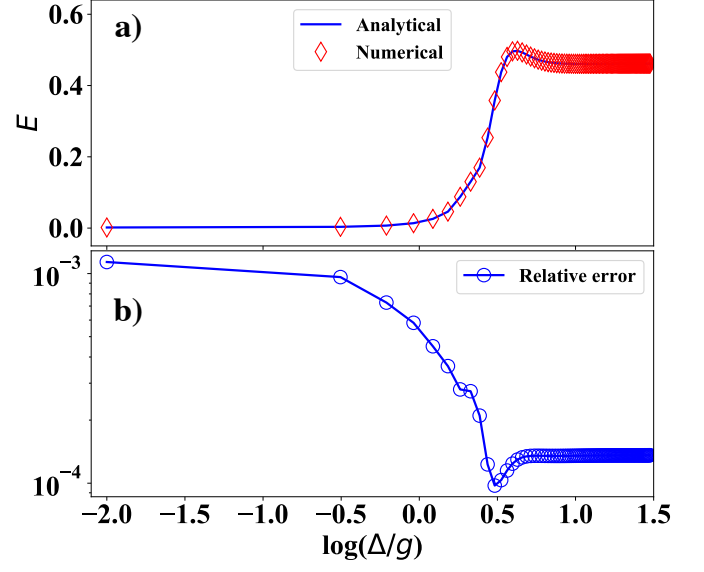


FIG. 4. (a) Time-averaged linear entropy E as a function of $\log_{10}(\Delta/g)$. (b) Comparison between the analytical and numerical predictions of E (cf. Eq. (9)). We use parameters $g = 10^{-2}\omega$, $J = 10^{-4}\omega$, where ω is the resonator frequency.

resonance condition $E_2^- - 2E_1^- = 0$ ($a = c$) (cf. Fig.2(b)). Also, $|b| = \sqrt{2}J$ and $\Omega = 4J$, so the asymptotic value of $\text{Var}(n_i)$ reads

$$\lim_{\Delta/g \rightarrow \infty} \text{Var}(n_i) = \frac{1}{2} \left(1 - \frac{1}{4} \sin 4 \right) = 0.5946. \quad (7)$$

It is worth mentioning that the analytical result (6) represents the hallmark for the dimer dynamics. In Sec. IV, we will prove that as one increases the number of lattice sites, the time-averaged variance (6) allows us to identify resonances due to intrinsic short- and long-range two-body interactions, which govern the DDP.

On the other hand, one can also characterize the dimer dynamics via the linear entropy of the reduced density matrix as mixedness measure [50]. First, notice that the quantum state (4) is already in its Schmidt decomposition, which leads to a diagonal reduced density matrix

$$\rho_i = \begin{pmatrix} |c_{2j}^-(t)|^2 & 0 & 0 \\ 0 & |c_0(t)|^2 & 0 \\ 0 & 0 & |c_{2i}^-(t)|^2 \end{pmatrix}. \quad (8)$$

In this case, the linear entropy as a function of time is given by $S_{\rho_i}(t) = 1 - (|c_0(t)|^4 + 2|c_{2i}^-(t)|^4)$, and the time-averaged linear entropy reads

$$E = \frac{2b^2}{\Omega_0^5} \left[2\Omega_0\Omega_1^2 - 4J\Omega_2^2 \sin\left(\frac{\Omega_0}{J}\right) - 3b^2J \sin\left(\frac{2\Omega_0}{J}\right) \right], \quad (9)$$

where $\Omega_1 = \sqrt{7b^2 + 2(a - c)^2}$ and $\Omega_2 = \sqrt{2b^2 + (a - c)^2}$. Figure 4(a) shows the behavior of E as a function of

$\log_{10}(\Delta/g)$ calculated from the full numerics (red diamonds) and the analytical prediction (continuous blue line) in Eq. (9). We see a good agreement between analytical and numerical predictions as shown in Fig. 4(b). We can also estimate the asymptotic value of the time-averaged entropy as one increases the ratio Δ/g , it reads

$$\lim_{\Delta/g \rightarrow \infty} E = 0.4616. \quad (10)$$

In what follows, we will use the time-averaged variance (6) for demonstrating the existence of DDP in the intermediate regime of light-matter interaction. This choice establishes the physical framework for the subsequent discussion, but a similar analysis with the linear entropy leads to the same conclusion about DDP.

IV. DYNAMICAL DIMERIZATION PHASE

Emergent dynamical critical phenomena following a quantum quench have experienced much interest in recent years [51, 52]. Termed as dynamical quantum phase transitions (DQPTs) [53–59], two classes have been identified depending on the type of quantum quench. The first class, DQPT-I [54, 60–68], describes a nonequilibrium critical phenomena where a time-averaged order parameter is non-zero in the long-time limit for quenches $\lambda_f < \lambda_c$, but vanishes for quenches across the critical point λ_c , i.e., $\lambda_f > \lambda_c > \lambda_i$. The second class, DQPT-II [53, 69–73], generalizes the notion of nonanalyticity in the free energy density to the nonequilibrium dynamics, based on the complex Loschmidt amplitude $\mathcal{G}(t) = \langle \psi(0) | e^{-i\hat{H}(\lambda_f)t} | \psi(0) \rangle$, which resembles the partition function $Z(\beta)$ in statistical mechanics.

In section III, we have fully described a particular quench dynamics of the Jaynes-Cummings dimer, which give rise to nonequilibrium critical phenomena, such as the transition from the Mott-insulating to superfluid phase. These simulated states are well described within the resonant (Mott-insulating) and dispersive (superfluid) regimes of light-matter interaction and the transition can be characterized via time-averaged order parameters such as the local variance $\text{Var}(n_i)$ and linear entropy E . Thus, the simulated nonequilibrium phenomena discussed in this work matches well within DQPT-I.

Here, we demonstrate an emergent *dynamical dimerization phase* as we extend the Jaynes-Cummings lattice to three (trimer) and four (tetramer) sites (cf. Fig.1), and in an intermediate regime of light-matter coupling strength, that is, $1 < \Delta/g < 10$. We define the concept of dimerization as the dynamical process where short-range and long-range two-body interactions govern the quantum dynamics. Here, short-range (long-range) two-body interaction is due to the direct (mediated) exchange of polaritons. We will prove that the connectivity associated with each node of the lattice plays a crucial role to define DDP.

Let us start the discussion with a three-sites JC lattice initialized in the state $|\psi_0\rangle = |1, -\rangle_i |1, -\rangle_j |1, -\rangle_k$, where the subindexes i, j , and k refer to the leftmost, center, and rightmost lattice site, respectively. If we let the system evolves according to the quantum quench described in Sec. III, one should impose the conditions for neglecting interchange of polaritonic species between nearest-neighbor sites, that is, $\{|E_2^+ - 2E_1^-, |2E_1^+ - E_2^-, |E_1^+ + E_1^- - E_2^-, |E_1^+ - E_1^-, |E_3^+ - E_2^- - E_1^-, |E_2^+ - E_2^-, |E_2^+ + E_1^+ - E_2^- - E_1^-\} \gg J$. As for the dimer, only the lower polaritonic branch will be activated and the dimension of the effective Hilbert space (\mathcal{H}) is given by $(N + d - 1)!/N!(d - 1)!$, where N is the number of excitations that should be distributed into d lattice sites. In our case, $N = 3$ and $d = 3$ results in $\dim(\mathcal{H}) = 10$. At time t , the wave function may be written as a linear combination of states belonging to the three-excitations subspace, that is,

$$\begin{aligned} |\psi(t)\rangle = & c_0(t)|\psi_0\rangle + c_{3j}|\psi_{3j}\rangle \\ & + c_{3i}(t)(|\psi_{3i}\rangle + |\psi_{3k}\rangle) \\ & + c_{2i1j}(t)(|\psi_{2i1j}\rangle + |\psi_{1j2k}\rangle) \\ & + c_{1i2j}(t)(|\psi_{1i2j}\rangle + |\psi_{2j1k}\rangle) \\ & + c_{2i1k}(t)(|\psi_{2i1k}\rangle + |\psi_{1i2k}\rangle), \end{aligned} \quad (11)$$

where we define states $|\psi_0\rangle = |1, -\rangle_i |1, -\rangle_j |1, -\rangle_k$, $|\psi_{3i}\rangle = |3, -\rangle_i |0, -\rangle_j |0, -\rangle_k$, $|\psi_{3j}\rangle = |0, -\rangle_i |3, -\rangle_j |0, -\rangle_k$, $|\psi_{3k}\rangle = |0, -\rangle_i |0, -\rangle_j |3, -\rangle_k$, $|\psi_{2i1j}\rangle = |2, -\rangle_i |1, -\rangle_j |0, -\rangle_k$, $|\psi_{1j2k}\rangle = |0, -\rangle_i |1, -\rangle_j |2, -\rangle_k$, $|\psi_{1i2j}\rangle = |1, -\rangle_i |2, -\rangle_j |0, -\rangle_k$, $|\psi_{2j1k}\rangle = |0, -\rangle_i |2, -\rangle_j |1, -\rangle_k$, $|\psi_{2i1k}\rangle = |2, -\rangle_i |0, -\rangle_j |1, -\rangle_k$, and $|\psi_{1i2k}\rangle = |1, -\rangle_i |0, -\rangle_j |2, -\rangle_k$. Notice that some probability amplitudes are equal due to symmetry of the trimer with respect to the lattice center (j). Here, the state (11) will be computed via full numerics.

Figure 5 shows the ratio between time-averaged nearest-neighbor correlation function C_{ij} (next nearest-neighbor correlation function C_{ik}) of the trimer, and the dimer variance (6). Two-point correlation functions are $C_{ij(k)} = \frac{1}{\tau} \int_0^\tau (\langle n_i n_j(k) \rangle - \langle n_i \rangle \langle n_j(k) \rangle) dt$, where $\tau = J^{-1}$. Here, we identify two critical values of detuning, vertical dashed lines, $\Delta/g = (2.43, 2.73)$ within the intermediate regime of light-matter interaction, $1 < \Delta/g < 10$. At these critical points the trimer experiences dynamical dimerization processes, where short-range correlations rule the dynamics at $\Delta/g = 2.43$, while at $\Delta/g = 2.73$ a combination of both short- and long-range correlations govern the dynamics. The resonances shown in Fig. 5 demonstrate that the intrinsic dimer dynamics, characterized by the time-averaged variance (6), governs the quench dynamics of the trimer. Furthermore, the dimer variance allows to identify short-range and long-range two-body interactions. The former is a consequence of direct cavity-cavity coupling of sites (i, k) , while the latter results from an indirect interaction between sites (i, k) mediated by the center lattice site j . Notice that Fig. 5 also exhibits an anti-resonance at $\Delta = 1.82g$ (continuous

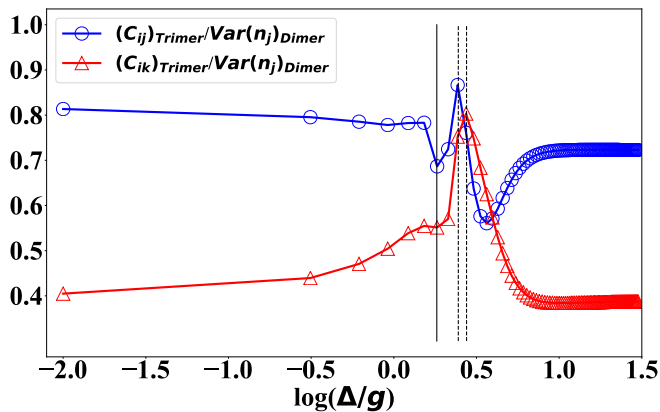


FIG. 5. Ratio between time-averaged nearest-neighbor correlation function C_{ij} (next nearest-neighbor correlation function C_{ik}) of the trimer, and the dimer variance in Eq. (6). Vertical dashed lines, from left to right, indicate critical values of detuning $\Delta/g = (2.43, 2.73)$ where dynamical dimerization processes happen. Continuous vertical line stands for the anti-resonance. We use parameters $g = 10^{-2}\omega$, $J = 10^{-4}\omega$, where ω is the resonator frequency, and we consider up to 5 Fock states per resonator.

vertical line). At this point, no dynamical dimerization happens and the JC lattice remains approximately in the Mott-insulating state.

Let us discuss the results for the tetramer. Figure 6 shows the ratio between time-averaged two-point correlation functions C_{ij} , C_{ik} , C_{il} of the tetramer, and the dimer variance in Eq. (6). We order the lattice sites from left to the right according to indexes (i, j, k, l) . It is noticeable that a larger JC lattice also exhibits resonances at critical values of detuning $\Delta/g = (2.43, 2.73)$ (vertical dashed lines), and the anti-resonance at $\Delta = 1.82g$ (continuous vertical line). Moreover, the two-point correlation function C_{il} , associated with edges of the lattice, has the same resonance ($\Delta = 2.43g$) as compared with nearest-neighbor correlation function C_{ij} . The latter suggests that for a finite one-dimensional JC lattice of L sites, the number of resonances associated with dimerization processes corresponds to a universal number of different connectivities of the lattice, that is, connectivity $\nu = 1$ for lattice edges, and connectivity $\nu = 2$ for bulk lattice sites. These results are a consequence of the broken translational symmetry.

V. CONCLUSIONS

In summary, we have reported on the emergence of a *dynamical dimerization phase* in a finite-sized Jaynes-Cummings lattice as a result of a quantum quench from an initial state with integer filling factor. We have thoroughly analyzed the quench dynamics in a two-sites Jaynes-Cummings lattice, which allows us to obtain analytical results for time-averaged order parameters such

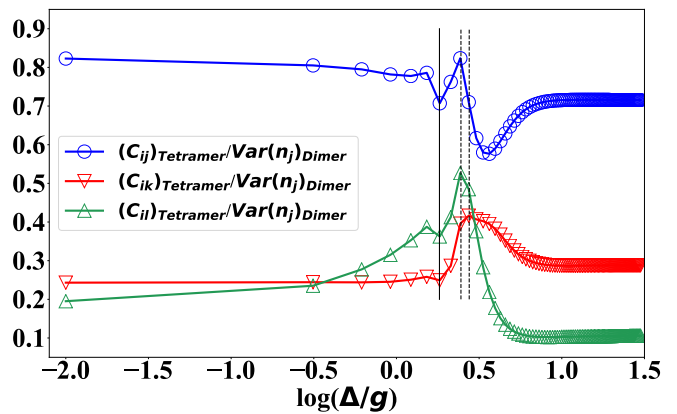


FIG. 6. Ratio between time-averaged two-point correlation functions C_{ij} , C_{ik} , C_{il} of the tetramer (four-sites JC lattice), and the dimer variance in Eq. (6). Vertical dashed lines, from left to right, indicate critical values of detuning $\Delta/g = (2.43, 2.73)$ where dynamical dimerization processes happen. Continuous vertical line stands for the anti-resonance. We use parameters $g = 10^{-2}\omega$, $J = 10^{-4}\omega$, where ω is the resonator frequency, and we consider up to 5 Fock states per resonator.

as the local variance of the number of polaritons, and the linear entropy. Further, these order parameters can be used to analyze and predict the resulting quenched dynamics for more complex architectures. When comparing dimer variance with two-point correlation functions of the trimer and tetramer, it allows us to determine critical values for the detuning where dynamical dimerization processes happen. Recognizing resonances and anti-resonance for detuning values, in turn, allow controlling what kind of correlation dominates over the dynamics be short-range or a combination of both short- and long-range, and may also allow controlling polariton propagation along the lattice. We stress that the intrinsic dimer dynamics, characterized by the time-averaged variance (6), governs the quench dynamics of finite-sized JC lattices, and we expect similar results as one increases the number of lattice sites. We conjecture that for a finite one-dimensional JC lattice of L sites, the number of resonances associated with dimerization processes corresponds to the number of different connectivities of the lattice, that is, connectivity $\nu = 1$ for lattice edges, and connectivity $\nu = 2$ for bulk lattice sites. Our findings could be tested with state-of-the-art quantum technologies. For instance, in trapped ions technology, the Jaynes-Cummings-Hubbard model has been theoretically proposed in Ref. [74] and physically implemented in Ref. [75]. In superconducting circuits, the JC dimer has been implemented in Ref. [15]. In this case, homodyne signal detection may allow measuring the local variance of photon number, which can also be used as an order parameter.

ACKNOWLEDGEMENTS

R. Peña acknowledges the support from Vicerrectoría de Postgrado USACH, F. Torres acknowledges financial support from grants FA9550-16-1-0122, FA9550-18-1-

0438, Fondecyt 1160639, and CEDENNA through the Financiamiento Basal para Centros Científicos y Tecnológicos de Excelencia-FB0807. G. Romero acknowledges the support from the Fondo Nacional de Desarrollo Científico y Tecnológico (FONDECYT) under grant No. 1190727.

-
- [1] Le Si Dang, D. Heger, R. André, F. Bœuf, and R. Romestain, “Stimulation of polariton photoluminescence in semiconductor microcavity,” *Phys. Rev. Lett.* **81**, 3920–3923 (1998).
- [2] P. Senellart, J. Bloch, B. Sermage, and J. Y. Marzin, “Microcavity polariton depopulation as evidence for stimulated scattering,” *Phys. Rev. B* **62**, R16263–R16266 (2000).
- [3] D. Porras, C. Ciuti, J. J. Baumberg, and C. Tejedor, “Polariton dynamics and bose-einstein condensation in semiconductor microcavities,” *Phys. Rev. B* **66**, 085304 (2002).
- [4] Guillaume Malpuech, Aldo Di Carlo, Alexey Kavokin, Jeremy J. Baumberg, Marian Zamfirescu, and Paolo Lugli, “Room-temperature polariton lasers based on gan microcavities,” *Applied Physics Letters* **81**, 412–414 (2002), <https://doi.org/10.1063/1.1494126>.
- [5] J. Kasprzak, M. Richard, S. Kundermann, A. Baas, P. Jeambrun, J. M. J. Keeling, F. M. Marchetti, M. H. Szymańska, R. André, J. L. Staehli, V. Savona, P. B. Littlewood, B. Deveaud, and Le Si Dang, “Bose–einstein condensation of exciton polaritons,” *Nature* **443**, 409–414 (2006).
- [6] P. G. Savvidis, J. J. Baumberg, R. M. Stevenson, M. S. Skolnick, D. M. Whittaker, and J. S. Roberts, “Angle-resonant stimulated polariton amplifier,” *Phys. Rev. Lett.* **84**, 1547–1550 (2000).
- [7] C. Ciuti, P. Schwendimann, B. Deveaud, and A. Quattropani, “Theory of the angle-resonant polariton amplifier,” *Phys. Rev. B* **62**, R4825–R4828 (2000).
- [8] M. Saba, C. Ciuti, J. Bloch, V. Thierry-Mieg, R. André, Le Si Dang, S. Kundermann, A. Mura, G. Bongiovanni, J. L. Staehli, and B. Deveaud, “High-temperature ultrafast polariton parametric amplification in semiconductor microcavities,” *Nature* **414**, 731–735 (2001).
- [9] Iacopo Carusotto and Cristiano Ciuti, “Probing microcavity polariton superfluidity through resonant rayleigh scattering,” *Phys. Rev. Lett.* **93**, 166401 (2004).
- [10] Alexey Kavokin, Guillaume Malpuech, and Fabrice P. Laussy, “Polariton laser and polariton superfluidity in microcavities,” *Physics Letters A* **306**, 187 – 199 (2003).
- [11] S. I. Tsintzos, N. T. Pelekanos, G. Konstantinidis, Z. Hatzopoulos, and P. G. Savvidis, “A gaas polariton light-emitting diode operating near room temperature,” *Nature* **453**, 372–375 (2008).
- [12] A Nunnenkamp, Jens Koch, and S M Girvin, “Synthetic gauge fields and homodyne transmission in jaynes–cummings lattices,” *New Journal of Physics* **13**, 095008 (2011).
- [13] Andrew A. Houck, Hakan E. Türeci, and Jens Koch, “On-chip quantum simulation with superconducting circuits,” *Nature Physics* **8**, 292–299 (2012).
- [14] D. L. Underwood, W. E. Shanks, Jens Koch, and A. A. Houck, “Low-disorder microwave cavity lattices for quantum simulation with photons,” *Phys. Rev. A* **86**, 023837 (2012).
- [15] J. Raftery, D. Sadri, S. Schmidt, H. E. Türeci, and A. A. Houck, “Observation of a dissipation-induced classical to quantum transition,” *Phys. Rev. X* **4**, 031043 (2014).
- [16] D. L. Underwood, W. E. Shanks, Andy C. Y. Li, Lamia Ateshian, Jens Koch, and A. A. Houck, “Imaging photon lattice states by scanning defect microscopy,” *Phys. Rev. X* **6**, 021044 (2016).
- [17] Mattias Fitzpatrick, Neereja M. Sundaresan, Andy C. Y. Li, Jens Koch, and Andrew A. Houck, “Observation of a dissipative phase transition in a one-dimensional circuit qed lattice,” *Phys. Rev. X* **7**, 011016 (2017).
- [18] Cyril Vaneph, Alexis Morvan, Gianluca Aiello, Mathieu Féchant, Marco Aprili, Julien Gabelli, and Jérôme Estève, “Observation of the unconventional photon blockade in the microwave domain,” *Phys. Rev. Lett.* **121**, 043602 (2018).
- [19] Ruichao Ma, Brendan Saxberg, Clai Owens, Nelson Leung, Yao Lu, Jonathan Simon, and David I. Schuster, “A dissipatively stabilized mott insulator of photons,” *Nature* **566**, 51–57 (2019).
- [20] Michele C. Collodo, Anton Potočnik, Simone Gasparinetti, Jean-Claude Besse, Marek Pechal, Mahdi Sameti, Michael J. Hartmann, Andreas Wallraff, and Christopher Eichler, “Observation of the crossover from photon ordering to delocalization in tunably coupled resonators,” *Phys. Rev. Lett.* **122**, 183601 (2019).
- [21] Yariv Yanay, Jochen Braumüller, Simon Gustavsson, William D. Oliver, and Charles Tahan, “Realizing the two-dimensional hard-core bose-hubbard model with superconducting qubits,” (2019), [arXiv:1910.00933 \[quant-ph\]](https://arxiv.org/abs/1910.00933).
- [22] P. Roushan, C. Neill, J. Tangpanitanon, V. M. Bastidas, A. Megrant, R. Barends, Y. Chen, Z. Chen, B. Chiaro, A. Dunsworth, A. Fowler, B. Foxen, M. Giustina, E. Jeffrey, J. Kelly, E. Lucero, J. Mutus, M. Neeley, C. Quintana, D. Sank, A. Vainsencher, J. Wenner, T. White, H. Neven, D. G. Angelakis, and J. Martinis, “Spectroscopic signatures of localization with interacting photons in superconducting qubits,” *Science* **358**, 1175–1179 (2017).
- [23] Dimitris G. Angelakis, Marcelo Franca Santos, and Sougato Bose, “Photon-blockade-induced mott transitions and xy spin models in coupled cavity arrays,” *Phys. Rev. A* **76**, 031805 (2007).
- [24] Michael J. Hartmann, Fernando G. S. L. Brandao, and Martin B. Plenio, “Strongly interacting polaritons in coupled arrays of cavities,” *Nat Phys* **2**, 849–855 (2006).
- [25] Andrew D. Greentree, Charles Tahan, Jared H. Cole, and Lloyd C. L. Hollenberg, “Quantum phase transitions of light,” *Nat Phys* **2**, 856–861 (2006).
- [26] Neil Na, Shoko Utsunomiya, Lin Tian, and Yoshihisa Yamamoto, “Strongly correlated polaritons in a

- two-dimensional array of photonic crystal microcavities,” *Phys. Rev. A* **77**, 031803 (2008).
- [27] Jens Koch and Karyn Le Hur, “Superfluid–mott-insulator transition of light in the jaynes-cummings lattice,” *Phys. Rev. A* **80**, 023811 (2009).
- [28] James Quach, Melissa I. Makin, Chun-Hsu Su, Andrew D. Greentree, and Lloyd C. L. Hollenberg, “Band structure, phase transitions, and semiconductor analogs in one-dimensional solid light systems,” *Phys. Rev. A* **80**, 063838 (2009).
- [29] James Q. Quach, Chun-Hsu Su, Andrew M. Martin, Andrew D. Greentree, and Lloyd C. L. Hollenberg, “Reconfigurable quantum metamaterials,” *Opt. Express* **19**, 11018–11033 (2011).
- [30] Arda Halu, Silvano Garnerone, Alessandro Vezzani, and Ginestra Bianconi, “Phase transition of light on complex quantum networks,” *Phys. Rev. E* **87**, 022104 (2013).
- [31] Joaquín Figueroa, José Rogan, Juan Alejandro Valdivia, Miguel Kiwi, Guillermo Romero, and Felipe Torres, “Nucleation of superfluid-light domains in a quenched dynamics,” *Scientific Reports* **8**, 12766 (2018).
- [32] Raul Coto, Miguel Orszag, and Vitalie Eremeev, “Self-trapping triggered by losses in cavity qed,” *Phys. Rev. A* **91**, 043841 (2015).
- [33] E. T. Jaynes and F. W. Cummings, “Comparison of quantum and semiclassical radiation theories with application to the beam maser,” *Proceedings of the IEEE* **51**, 89–109 (1963).
- [34] Matthew P. A. Fisher, Peter B. Weichman, G. Grinstein, and Daniel S. Fisher, “Boson localization and the superfluid-insulator transition,” *Phys. Rev. B* **40**, 546–570 (1989).
- [35] S. Schmidt and G. Blatter, “Strong coupling theory for the jaynes-cummings-hubbard model,” *Phys. Rev. Lett.* **103**, 086403 (2009).
- [36] Davide Rossini and Rosario Fazio, “Mott-insulating and glassy phases of polaritons in 1d arrays of coupled cavities,” *Phys. Rev. Lett.* **99**, 186401 (2007).
- [37] Davide Rossini, Rosario Fazio, and Giuseppe Santoro, “Photon and polariton fluctuations in arrays of QED-cavities,” *EPL (Europhysics Letters)* **83**, 47011 (2008).
- [38] Adam G. D’Souza, Barry C. Sanders, and David L. Feder, “Fermionized photons in the ground state of one-dimensional coupled cavities,” *Phys. Rev. A* **88**, 063801 (2013).
- [39] Jian Xue, Kangjun Seo, Lin Tian, and Tao Xiang, “Quantum phase transition in a multiconnected jaynes-cummings lattice,” *Phys. Rev. B* **96**, 174502 (2017).
- [40] T Grujic, S R Clark, D Jaksch, and D G Angelakis, “Non-equilibrium many-body effects in driven nonlinear resonator arrays,” *New Journal of Physics* **14**, 103025 (2012).
- [41] Guifré Vidal, “Efficient simulation of one-dimensional quantum many-body systems,” *Phys. Rev. Lett.* **93**, 040502 (2004).
- [42] Michael Zwolak and Guifré Vidal, “Mixed-state dynamics in one-dimensional quantum lattice systems: A time-dependent superoperator renormalization algorithm,” *Phys. Rev. Lett.* **93**, 207205 (2004).
- [43] C. D. Ogden, E. K. Irish, and M. S. Kim, “Dynamics in a coupled-cavity array,” *Phys. Rev. A* **78**, 063805 (2008).
- [44] M. I. Makin, Jared H. Cole, Charles D. Hill, Andrew D. Greentree, and Lloyd C. L. Hollenberg, “Time evolution of the one-dimensional jaynes-cummings-hubbard hamiltonian,” *Phys. Rev. A* **80**, 043842 (2009).
- [45] R Chakrabarti and G Sreecumari, “Propagation of single-excitation quantum states through jaynes-cummings-hubbard arrays,” *Journal of Physics B: Atomic, Molecular and Optical Physics* **44**, 115505 (2011).
- [46] Raul Coto and Miguel Orszag, “Propagation and distribution of quantum correlations in a cavity QED network,” *Journal of Physics B: Atomic, Molecular and Optical Physics* **46**, 175503 (2013).
- [47] James Q. Quach, “Disorder-correlation-frequency-controlled diffusion in the jaynes-cummings-hubbard model,” *Phys. Rev. A* **88**, 053843 (2013).
- [48] J.R. Johansson, P.D. Nation, and Franco Nori, “Qutip: An open-source python framework for the dynamics of open quantum systems,” *Computer Physics Communications* **183**, 1760 – 1772 (2012).
- [49] J.R. Johansson, P.D. Nation, and Franco Nori, “Qutip 2: A python framework for the dynamics of open quantum systems,” *Computer Physics Communications* **184**, 1234 – 1240 (2013).
- [50] Giuliano Benenti, Giulio Casati, Davide Rossini, and Giuliano Strini, *Principles of Quantum Computation and Information* (WORLD SCIENTIFIC, 2018) <https://www.worldscientific.com/doi/pdf/10.1142/10909>.
- [51] Markus Heyl, “Dynamical quantum phase transitions: a review,” *Reports on Progress in Physics* **81**, 054001 (2018).
- [52] Markus Heyl, “Dynamical quantum phase transitions: A brief survey,” *EPL (Europhysics Letters)* **125**, 26001 (2019).
- [53] M. Heyl, A. Polkovnikov, and S. Kehrein, “Dynamical quantum phase transitions in the transverse-field ising model,” *Phys. Rev. Lett.* **110**, 135704 (2013).
- [54] Bojan Žunkovič, Markus Heyl, Michael Knap, and Alessandro Silva, “Dynamical quantum phase transitions in spin chains with long-range interactions: Merging different concepts of nonequilibrium criticality,” *Phys. Rev. Lett.* **120**, 130601 (2018).
- [55] Jad C. Halimeh and Valentin Zauner-Stauber, “Dynamical phase diagram of quantum spin chains with long-range interactions,” *Phys. Rev. B* **96**, 134427 (2017).
- [56] Valentin Zauner-Stauber and Jad C. Halimeh, “Probing the anomalous dynamical phase in long-range quantum spin chains through fisher-zero lines,” *Phys. Rev. E* **96**, 062118 (2017).
- [57] Ingo Homrighausen, Nils O. Abeling, Valentin Zauner-Stauber, and Jad C. Halimeh, “Anomalous dynamical phase in quantum spin chains with long-range interactions,” *Phys. Rev. B* **96**, 104436 (2017).
- [58] Johannes Lang, Bernhard Frank, and Jad C. Halimeh, “Concurrence of dynamical phase transitions at finite temperature in the fully connected transverse-field ising model,” *Phys. Rev. B* **97**, 174401 (2018).
- [59] Jad C. Halimeh, Maarten Van Damme, Valentin Zauner-Stauber, and Laurens Vanderstraeten, “Quasiparticle origin of dynamical quantum phase transitions,” (2018), [arXiv:1810.07187 \[cond-mat.str-el\]](https://arxiv.org/abs/1810.07187).
- [60] Michael Moeckel and Stefan Kehrein, “Interaction quench in the hubbard model,” *Phys. Rev. Lett.* **100**, 175702 (2008).
- [61] Michael Moeckel and Stefan Kehrein, “Crossover from adiabatic to sudden interaction quenches in the hubbard model: prethermalization and non-equilibrium dynam-

- ics,” *New Journal of Physics* **12**, 055016 (2010).
- [62] Bruno Sciola and Giulio Biroli, “Quantum quenches and off-equilibrium dynamical transition in the infinite-dimensional bose-hubbard model,” *Phys. Rev. Lett.* **105**, 220401 (2010).
- [63] A. Gambassi and P. Calabrese, “Quantum quenches as classical critical films,” *Europhys. Lett.* **95**, 66007 (2011).
- [64] Bruno Sciola and Giulio Biroli, “Quantum quenches, dynamical transitions, and off-equilibrium quantum criticality,” *Phys. Rev. B* **88**, 201110 (2013).
- [65] Anna Maraga, Alessio Chiochetta, Aditi Mitra, and Andrea Gambassi, “Aging and coarsening in isolated quantum systems after a quench: Exact results for the quantum $O(n)$ model with $n \rightarrow \infty$,” *Phys. Rev. E* **92**, 042151 (2015).
- [66] Takashi Mori, Tatsuhiko N Ikeda, Eriko Kaminishi, and Masahito Ueda, “Thermalization and prethermalization in isolated quantum systems: a theoretical overview,” *Journal of Physics B: Atomic, Molecular and Optical Physics* **51**, 112001 (2018).
- [67] J. Zhang, G. Pagano, P. W. Hess, A. Kyprianidis, P. Becker, H. Kaplan, A. V. Gorshkov, Z. X. Gong, and C. Monroe, “Observation of a many-body dynamical phase transition with a 53-qubit quantum simulator,” *Nature* **551**, 601 (2017).
- [68] Jad C. Halimeh, Valentin Zauner-Stauber, Ian P. McCulloch, Inés de Vega, Ulrich Schollwöck, and Michael Kastner, “Prethermalization and persistent order in the absence of a thermal phase transition,” *Phys. Rev. B* **95**, 024302 (2017).
- [69] C. Karrasch and D. Schuricht, “Dynamical phase transitions after quenches in nonintegrable models,” *Phys. Rev. B* **87**, 195104 (2013).
- [70] F. Andraschko and J. Sirker, “Dynamical quantum phase transitions and the loschmidt echo: A transfer matrix approach,” *Phys. Rev. B* **89**, 125120 (2014).
- [71] P. Jurcevic, H. Shen, P. Hauke, C. Maier, T. Brydges, C. Hempel, B. P. Lanyon, M. Heyl, R. Blatt, and C. F. Roos, “Direct observation of dynamical quantum phase transitions in an interacting many-body system,” *Phys. Rev. Lett.* **119**, 080501 (2017).
- [72] Lorenzo Piroli, Balázs Pozsgay, and Eric Vernier, “Non-analytic behavior of the loschmidt echo in xxz spin chains: Exact results,” *Nuclear Physics B* **933**, 454 – 481 (2018).
- [73] Johannes Lang, Bernhard Frank, and Jad C. Halimeh, “Dynamical quantum phase transitions: A geometric picture,” *Phys. Rev. Lett.* **121**, 130603 (2018).
- [74] P. A. Ivanov, S. S. Ivanov, N. V. Vitanov, A. Mering, M. Fleischhauer, and K. Singer, “Simulation of a quantum phase transition of polaritons with trapped ions,” *Phys. Rev. A* **80**, 060301 (2009).
- [75] Kenji Toyoda, Yuta Matsuno, Atsushi Noguchi, Shinsuke Haze, and Shinji Urabe, “Experimental realization of a quantum phase transition of polaritonic excitations,” *Phys. Rev. Lett.* **111**, 160501 (2013).